Geophysical Research Letters

RESEARCH LETTER
10.1029/2021GL092537

Key Points:

- Gravity waves (GWs) at 20–70 km altitudes decreased after the onset of the 2019 Antarctic stratospheric sudden warming
- The decline of GW activity coincided with the weakening of zonal wind
- The decline in GW activity was caused by wind filtering, wave saturation, and disruption of the polar night jet

Supporting Information:

Supporting Information may be found in the online version of this article.

Correspondence to:

M. Kogure,
kogure.masaru.695@m.kyushu-u.ac.jp

Citation:

Kogure, M., Yue, J., & Liu, H. (2021). Gravity wave weakening during the 2019 Antarctic stratospheric sudden warming. *Geophysical Research Letters*, *48*, e2021GL092537. https://doi.org/10.1029/2021GL092537

Received 14 JAN 2021
Accepted 30 MAR 2021

Gravity Wave Weakening During the 2019 Antarctic Stratospheric Sudden Warming

Masaru Kogure[1], Jia Yue[2,3], and Huixin Liu[1]

[1]Department of Earth and Planetary Science, Kyushu University, Fukuoka, Japan, [2]NASA Goddard Space Flight Center, Greenbelt, MD, USA, [3]Physics Department, Catholic University of America, Washington, DC, USA

Abstract A rare Antarctic stratospheric sudden warming (SSW) occurred on August 30, 2019, and was a minor warming event. We investigated variations in gravity wave (GW) activity before and after this Antarctic SSW event using two satellite measurements (AIRS and CIPS) and reanalysis data (GEOS-5 FP). GW activity over the Andes decreased after August 30, although the westerly wind was 40–60 ms^{-1} and cannot filter out GWs with small zonal phase speed. This decline over the Andes was probably caused by wave saturation. Zonal mean GW activity over Antarctica and the Southern Ocean likewise decreased, with a weakening of zonal wind. The zonal mean GW activity further decreased around September 8 which coincided with a reversal of the zonal mean zonal wind at 40 km. The decline in the zonal mean GW activity after August 30 was probably caused by wind filtering and polar night jet breaking.

Plain Language Summary A strong westerly wind, called the polar night jet, appears in the winter polar region and typically exceeds 90 ms^{-1} at its maximum. The temperature inside the jet (the polar vortex) is colder than that outside the jet. However, the polar night jet occasionally becomes highly distorted and disappears with accompanying warming in the polar stratosphere. Such events are called sudden stratospheric warmings (SSWs). SSWs drastically change the wind and temperature, which should strongly influence small-scale waves, called gravity waves (GWs). SSWs frequently occur in the Arctic, but rarely in the Antarctic. Antarctic SSWs have occurred only twice in the 21st century. The rare Antarctic SSW occurred in 2019, and we investigated GW variations before/after the SSW event. A decline in GW activity coincided with a decline in the zonal wind twice in GEOS-5 FP. The decline in GW activity was probably caused by a weak zonal wind layer. This temporal variation is the same as the Arctic GWs for the same type of SSW.

1. Introduction

The winter polar stratosphere is characterized by a strong westerly wind, i.e., the polar night jet (Chandran et al., 2014). The polar night jet exceeds 90 ms^{-1}, and the temperature inside the jet (the polar vortex) is colder than that outside the jet (Fleming et al., 1990). However, the polar night jet occasionally becomes highly distorted and sometimes disappears with accompanying warming. Such events are called sudden stratospheric warmings (SSWs). SSWs are triggered by enhanced propagation of wavenumber one or two planetary waves from the troposphere, and planetary wave breaking decelerates the polar night jet and sometimes reverses the zonal wind (Chandran et al., 2014).

The World Meteorological Organization classifies SSWs into two categories: minor and major warmings. During minor warmings, the zonal mean temperature at the pole is higher than that at 60°N at 10 hPa. During a major warming, the zonal wind reverses from a westerly wind to an easterly wind at 10 hPa, in addition to higher temperatures at the pole (Chandran et al., 2014). Furthermore, SSWs can be categorized by their zonal structures, polar vortex displacement, or splitting events (Charlton & Polvani, 2007; Matthewman et al., 2009). During a vortex displacement event, the vortex moves out of the pole and tilts westward with height, with an enhanced wavenumber 1 planetary wave. During a vortex splitting event, the vortex splits into two or more cyclonic cells, with an enhanced wavenumber 2 planetary wave.

Because SSWs drastically change the meteorological fields in the middle atmosphere, gravity wave (GW) generation and propagation are consequently altered. SSW effects on GWs in the northern hemisphere have been well studied due to the frequent occurrence of Antarctic SSWs. Ern et al. (2016) investigated temporal Arctic GW variations before and after SSW onsets from 2001 to 2014 and showed that GW activity

was strongly suppressed when the zonal wind reversed after the onset. Ern et al. (2016) also found that the GW activity was enhanced prior to SSW onset when major warmings and split vortex events occurred and could be caused by increased imbalance in the flow. These characteristics of Arctic GWs during SSWs have been supported by models and observational studies (Jia et al., 2015; Thurairajah et al., 2014; Wang & Alexander, 2009; Wright et al., 2010; Yamashita et al., 2010, 2013). In contrast, Antarctic SSWs have occurred only twice in the 21st century (2002 and 2019). Most satellite observations of GWs became available after 2000. The 2002 Antarctic SSW was a vortex splitting major warming event (Baldwin et al., 2003). Ratnam et al. (2004) used CHAMP/GPS occultation measurements to determine that the enhancement and decline of Antarctic GW activity occurred before and after the SSW onset, respectively. This is consistent with the Arctic vortex splitting major warming events. The 2019 Antarctic SSW occurred around August 30 and was led by the enhancement of planetary waves with zonal wavenumber 1 (Yamazaki et al., 2020). Although this 2019 SSW event was classified as a minor warming event, the zero zonal wind layer reached 40 km, which could create critical levels for GWs with small zonal phase speed and influence GW activity in the southern hemisphere. The objective of this study was to reveal temporal and spatial GW variations in the southern hemisphere before and after the 2019 Antarctic SSW event.

2. Analysis and Data

2.1. GEOS-5 FP

The GW perturbations and absolute momentum fluxes during the Antarctic 2019 SSW were estimated with the GEOS-5 FP (Forward Processing) reanalysis data (Lucchesi, 2013). The GEOS-5 FP is a global nonhydrostatic, high horizontal resolution $\left(0.3125^\circ \text{ longitude} \times 0.25^\circ \text{ latitude}\right)$ simulation, and is assimilated with observations. The GEOS-5 FP output used is the three-hourly interval instantaneous product and has 72 vertical levels from the surface to 0.01 hPa (~80 km). The vertical resolution was ~2 km in the middle atmosphere. The three top layers (0.01–0.04 hPa) are strong sponge layers; therefore, only GWs below 0.05 hPa (~70 km) were considered. The orographic and nonorographic GW parameterizations (Garcia & Boville, 1994; McFarlane, 1987) are also used in the GEOS-5 FP; however, in this study, we focused on resolved GWs in the GEOS-5 FP, that is, the GWs with horizontal and vertical wavelengths longer than ~100 and ~4 km, respectively. It should be noted that the amplitudes of GWs with smaller horizontal wavelengths (~100 km) can be significantly underestimated because of strong model damping (Gelaro et al., 2017).

To derive GW perturbations in the GEOS-5 FP, the background field was defined as a sum of spherical harmonic series up to horizontal wavenumber $n = 40$, which implies that the background field is composed of phenomena with horizontal wavelength longer than ~1,000 km, according to Holt et al. (2017). The GW perturbations were then obtained by subtracting the background. Thus, we derived GWs with horizontal wavelengths less than ~1,000 km. From the perturbations and background, the daily mean absolute GW momentum flux was estimated as in Equation 1 in Geller et al. (2013).

2.2. Atmospheric Infrared Sounder (AIRS)

The AIRS instrument aboard the NASA Aqua satellite (Aumann et al., 2003; Chahine et al., 2006) measures infrared radiance spectra between 3.74 and 15.4 μm. To investigate GWs, 15 μm brightness temperature data averaged over two sets of AIRS channels were used and compared with the GWs in GEOS-5 FP. The two channel sets were used for averaging, with temperature kernel functions peaking in two layers at ~23 and ~40 km. The full widths at half maximum of the kernel functions are typically ~15 km and therefore represent mean temperatures over 17–32 and 34–49 km, respectively. Second, a fourth-order polynomial fit was subtracted for each across-track scan to remove the backgrounds. The remaining temperature perturbations provided a measure of GWs with vertical wavelengths longer than ~15 km and ~30–500 km horizontal wavelengths. The AIRS/Aqua observations of GWs are described in detail by Hoffmann et al. (2013, 2017).

2.3. Cloud Imaging and Particle Size Instrument (CIPS)

The CIPS instrument on the NASA Aeronomy of Ice in the Mesosphere (AIM) (McClintock et al., 2009; Rusch et al., 2017) is a nadir-viewing panoramic imager that observes ultraviolet radiation (265 nm)

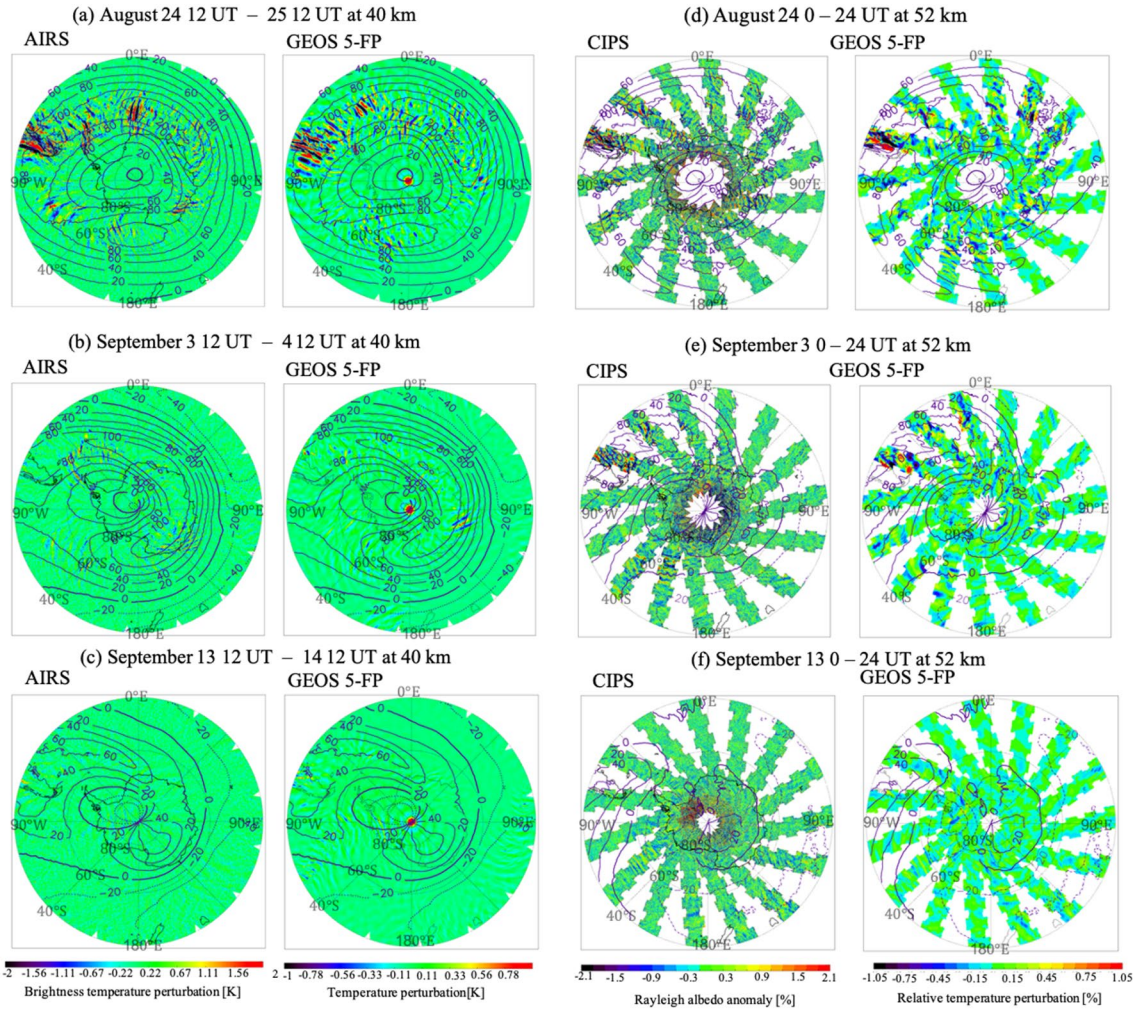

Figure 1. Graphs (a–c) show the gravity wave (GW) brightness temperature and temperature perturbations at ~40 km for AIRS and GEOS-5 FP in the Southern hemisphere (40°S–90°S) from 12 UT on August 24 to 12 UT on August 25, from 12 UT on September 3 to 12 UT on September 4, and from 12 UT on September 13 to 12 UT on September 14, respectively. Thick lines and dotted lines indicate 0 ms^{-1} and an easterly wind, respectively. Graphs (d–f) are same as (a-c), but show Rayleigh albedo anomalies for CIPS and relative temperature perturbations for GEOS-5 FP at ~52 km.

scattered by Rayleigh scattering and polar mesospheric clouds (PMCs). In the absence of PMCs (including the Antarctic region during austral winter), the Rayleigh scattering source function at the 265 μm radiance peaks at altitudes of 50–55 km, with ~15 km full width at a half maximum altitude (Bailey et al., 2009).

The Rayleigh scattering Albedo Anomaly (RAA) observed by CIPS corresponds to GW temperature relative perturbations (Randall et al., 2017). To calculate RAA, a background Rayleigh albedo was calculated using a numerical generalization of the "C – σ" model, which was described by Carstens et al. (2013). The RAA observed by the CIPS instrument is most sensitive to GWs at ~52 km, with vertical wavelengths longer than ~15 km and ~15–600 km horizontal wavelengths. RAA retrieval was described by Randall et al. (2017).

3. Time Variation of GW Temperature Perturbation in AIRS and CIPS Observations and the GEOS 5-FP Model

Figure 1 shows the GWs temperature perturbations observed by AIRS, CIPS and GEOS-5 FP. To compare observations with model simulations, the perturbations in the GEOS-5 FP were vertically averaged using the AIRS and CIPS observational vertical kernels with 15 km full width half maximum. The GW perturbations at 40 and 52 km (where the kernel functions peak) before the SSW onset (August 24) were large

over the Andes, the Antarctic peninsula (which are well known as orographic GW hot spots (Hoffmann et al., 2013), and the Southern Ocean. The area of GW enhancement over the Southern Ocean corresponds with the location of the polar night jet suggesting it could be the source of these GWs. Storm systems and fronts are other sources for the GWs over the Southern Ocean (Hendricks. et al., 2014). The GW perturbations after the SSW onset (September 3 and 13) were much weaker than those on August 24. The daily mean zonal wind in GEOS-5 FP also decreased after the SSW onset at ∼40 and ∼52 km. The vortex moved out of the pole toward the Andes, because the 2019 Antarctic SSW was a vortex displacement event. The GWs on September 3 still appeared over the Andes and Antarctic Peninsula, but the GWs have almost disappeared by September 3. Accompanying the decline of the perturbations, the zonal wind weakened and changed to an easterly wind, although the local zonal wind around the Andes was still a ∼30–60 m s^{-1} westerly wind. The GW perturbations at 23 km also decreased similar to those at 40 and 52 km, although the polar night jet remained (see Figure S1 in supporting information). Thus, the observed GW activity decreased after the SSW onset. Such a decline in the GWs during Arctic SSWs is well known and can be explained by three mechanisms: (a) wind filtering of GWs with small zonal phase velocities because of wind reversal (Ratnam et al., 2004; Yamashita et al., 2010), (b) weakening or even the disappearance of the GW sources, i.e., the polar night jet (Yamashita et al., 2010), (c) dissipation for GWs with larger amplitudes and shorter vertical wavelengths (Lindzen et al., 1981). Moreover, there is a possibility that an observational filter was applied because of the shortened vertical wavelengths (M. J. Alexander, 1998). However, observational filtering alone cannot explain this decrease because temperature perturbations in GEOS-5 FP without the kernel function applied also decreased (not shown).

It should be noted in Figure 1 that the amplitudes of the GWs in the observations were approximately two times larger than those in the model. Although the observations and the model are sensitive to GWs with longer and shorter wavelengths, respectively, the GWs with longer wavelengths typically have larger amplitudes than shorter ones (Fritts & Alexander, 2003). This underestimation of the amplitude in the GEOS-5 model has been reported by Holt et al. (2016, 2017) and is caused by the excessive dissipation because of the coarser vertical resolution. This is common in many general circulation models (Jewtoukoff et al., 2015).

Nevertheless, the GWs in GEOS-5 FP are in good agreement with the satellite observations in terms of their spatial and temporal variations although there are some discrepancies (e.g., the GWs around 0°E, 60°S in Figure 1a). Additionally, the analysis of GEOS-5 FP does not have observational filtering problems. We focus on the GWs in GEOS-5 FP during the Antarctic SSW in the following section.

4. Temporal and Special Variations of Absolute GW Momentum Fluxes in GEOS-5 FP Before and After the Antarctic 2019 SSW

Figures 2a and 2b show the zonal mean absolute GW momentum flux averaged over 50°S–70°S during 2018 and 2019, respectively. Figures 2c, 2d, and 2e show the flux averaged in 15–25, 35–45, and 55–65 km altitudes. No Antarctic SSW occurred in 2018, and the flux in 2018 was typical and is shown as a reference. In 2019, the flux before the onset (August 30, 2019) was comparable with that in 2018. After the onset, the fluxes at the 35–45 and 55–65 km altitudes on August 30 decreased by half of that during August 20–29. The fluxes in 35–45 km and 55–65 km altitudes on September 12–19 were twice and seven times smaller than that during August 20–29, respectively. The zonal wind became weaker above ∼25 km at the SSW onset but there was still a westerly wind. On September 5, the zero zonal wind line dropped to ∼40 km (3 hPa). Thus, the flux and zonal wind in 2019 were smaller above ∼35 km than those in 2018. This temporal variation was different from the 2002 Antarctic splitting vortex SSW, because no GW enhancement occurred before the SSW onset (Ratnam et al., 2004), but was similar to the Arctic GWs during vortex displacement minor SSWs (Ern et al., 2016).

To investigate the spatial variations in the absolute GW momentum fluxes, we calculated the fluxes averaged over three periods: before the SSW onset (August 20–29), after the SSW but while the zonal wind was still westerly at a 40 km (August 30–September 8), and when the zonal wind was easterly at 40 km (September 9–19). Figure 3 shows the absolute GW momentum fluxes over 40°S–90°S at 100, 10, 1, and 0.1 hPa (15, 30, 47, and 64 km) during the three periods, respectively. The flux at 100 hPa in ($0°\mathrm{E} - 135°\mathrm{W}, \geq 40°\mathrm{S}$) decreased to ∼40% from August 20–29 (Figure 3a) to September 9–19 (Figure 3c), which could be caused by

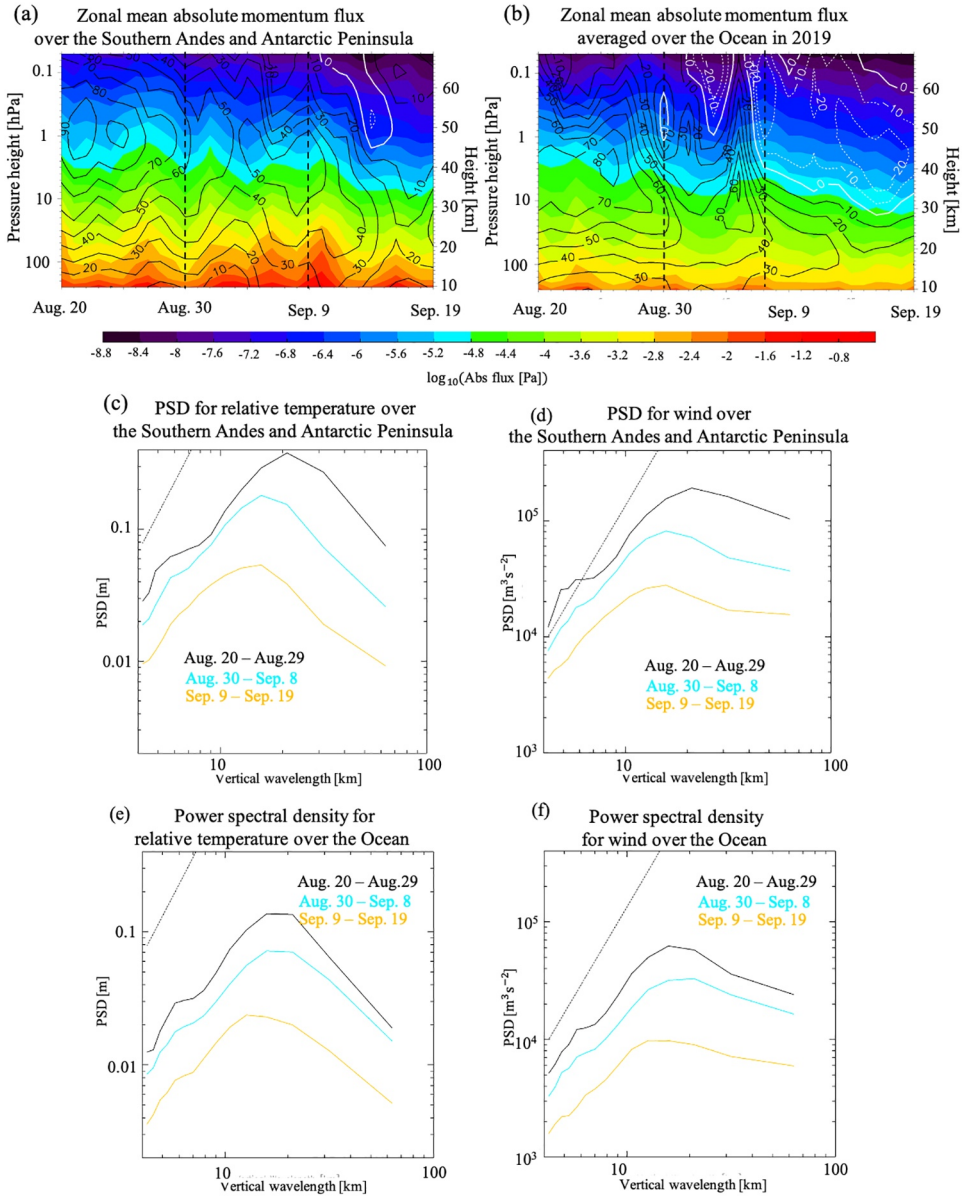

Figure 2. Graphs (a and b) show the daily mean absolute momentum fluxes in GEOS-5 FP over 50°W–80°W, 50°S–70°S (the southern Andes and Antarctic peninsula) and 165°E—165°W, 50°S–70°S (hereinafter, this region is called the ocean region). Graphs (c and d) show the vertical wavelength power spectral densities (PSDs) for the gravity wave (GW) relative temperature and wind perturbation over the southern Andes and Antarctic peninsula in 10–70 km during August 20–30 (black), August 31–September 8 (blue), and September 9–19 (orange), respectively. Graphs (e and f) are the same as that in (c), except over the ocean region. The dashed line indicated theoretical saturated spectrum for $N^2 = 4 \times 10^{-4}$ s^{-2}.

the weaker source (the polar night jet). An area where zonal wind was larger than $40\ \mathrm{ms}^{-1}$ at 100 hPa was likewise shrunk from August 20–29 (Figure 3a) to September 9–19 (Figure 3c). At 10 hPa, the fluxes on 20–29 August (Figure 3d) were high around the polar night jet (50°S–70°S), the Andes, and the Antarctic peninsula, which is a typical special variation during austral winter (Preusse et al., 2009). Additionally, the high GW flux region over the Andes extended leeward (up to ~40°W in Figure 3d). During August 30–September 8 (Figure 3e), the polar night jet weakened and shrank, and the flux around the polar night jet decreased by approximately half (Figure 3e). Between September 9–19 (Figure 3f), the polar night jet weakened and shrunk more, and the flux also further decreased in the eastern hemisphere. It should be noted that the flux

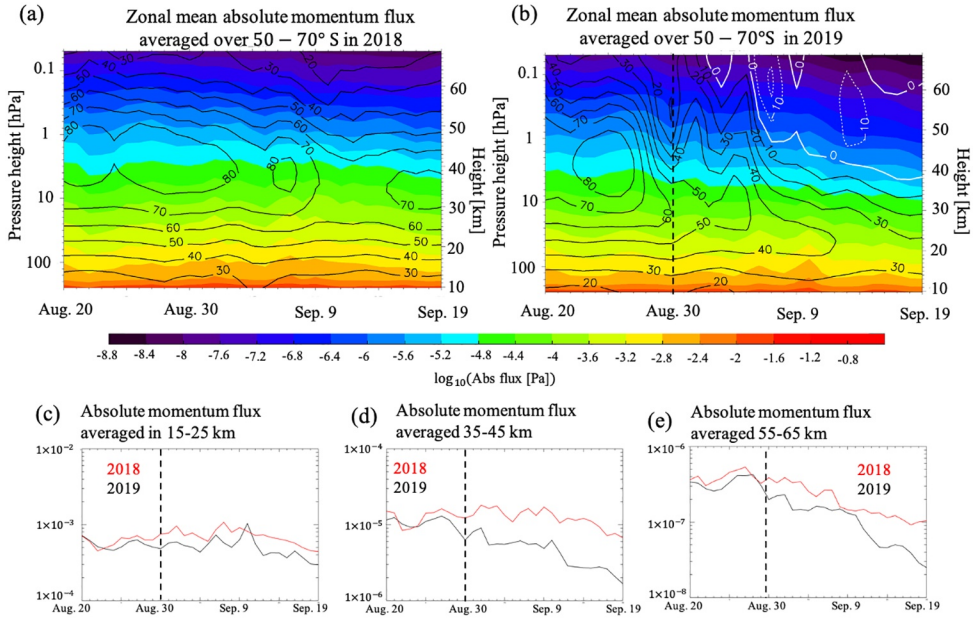

Figure 3. Daily mean absolute momentum fluxes in GEOS 5-FP over 50°S–70°S. Graphs (a and b) show the zonal mean fluxes in 2018 and 2019, respectively. Contour lines indicate daily mean zonal wind. Thick, solid, and dotted lines indicate a 0 ms^{-1}, westerly, and easterly wind, respectively. Graphs (c, d, and e) show absolute momentum fluxes averaged in 15–25, 35–45, and 55–65 km altitudes, respectively. The dot lines indicate the stratospheric sudden warming (SSW) onset.

in the red box of Figure 3f was larger during September 9–19 than those during August 20–29 and August 30–September 8. This area overlapped with an exit region of the polar night jet, and consequently, the GWs could be emitted from the polar night jet through spontaneous adjustment (Plougonven & Zhang, 2014). The temporal variations of flux and zonal wind at 1 and 0.1 hPa were also similar to those at 10 hPa, but the jet disappeared at 1 and 0.1 hPa (Figure 3i and 3l). The flux dropped by 1–2 orders in the polar night jet region (50°S–60°S), the Andes, and the Antarctic peninsula from August 20–29 (Figures 3g and 3j) to September 9–19 (Figures 3i and 3l). The zonal winds around the Andes and the Antarctic peninsula were mostly westerly after the onset (Figures 3f and 3i), but the ones over most regions of the Southern Ocean, especially in the eastern hemisphere, were easterly. A main source of GWs in the Andes and the Antarctic peninsula is wind flowing over mountains, whereas the main sources over the Southern Ocean should be fronts and the polar night jet (Hendricks et al., 2014; Murphy et al., 2014; Sato & Yoshiki, 2008). Thus, the behavior of the GWs and the background winds in both regions were different. We compare the GW fluxes between the Andes and the Antarctic peninsula and the Southern Ocean in the following paragraph.

Figures 4a and 4b show the daily mean absolute momentum fluxes in GEOS-5 FP over 50°W–80°W, 50°S–70°S (upper black box in Figure 3d, i.e., the Andes and the Antarctic peninsula, and 165°E–165°W, 50°S–70°S (lower black box in Figure 3d (hereinafter, this region is called the ocean region). The ocean region is far from any continent, and the polar night jet existed there before the onset, although there are three small islands (Balleny, Auckland, and Macquarie) that produce local GW momentum flux (M. J. Alexander & Grimsdell, 2013; Hoffmann et al., 2016). Thus, the contribution of nonorographic GWs to the flux should be much larger than that over the southern Andes and Antarctic peninsula. The wind and flux over the ocean region were similar to the zonal mean values in Figure 3b (e.g., zonal wind peak altitude and the time of the decline of the zonal wind and the flux), although the flux was twice smaller than the zonal mean value. This is because most areas in 50°S–70°S are over the ocean. The flux over the southern Andes and Antarctic peninsula was 10%–50% larger than the zonal mean value, especially in the lower stratosphere. This high flux was caused by mountain waves. In terms of temporal variations, the zonal wind and flux in both regions decreased in two periods (the first period was the SSW onset, i.e., August 30, and the second was the drop in the zonal wind, i.e., September 7 and 9 in the Ocean region and the southern Andes and Antarctic peninsula, respectively). The weakening zonal wind coinciding with the decrease of the flux suggests that

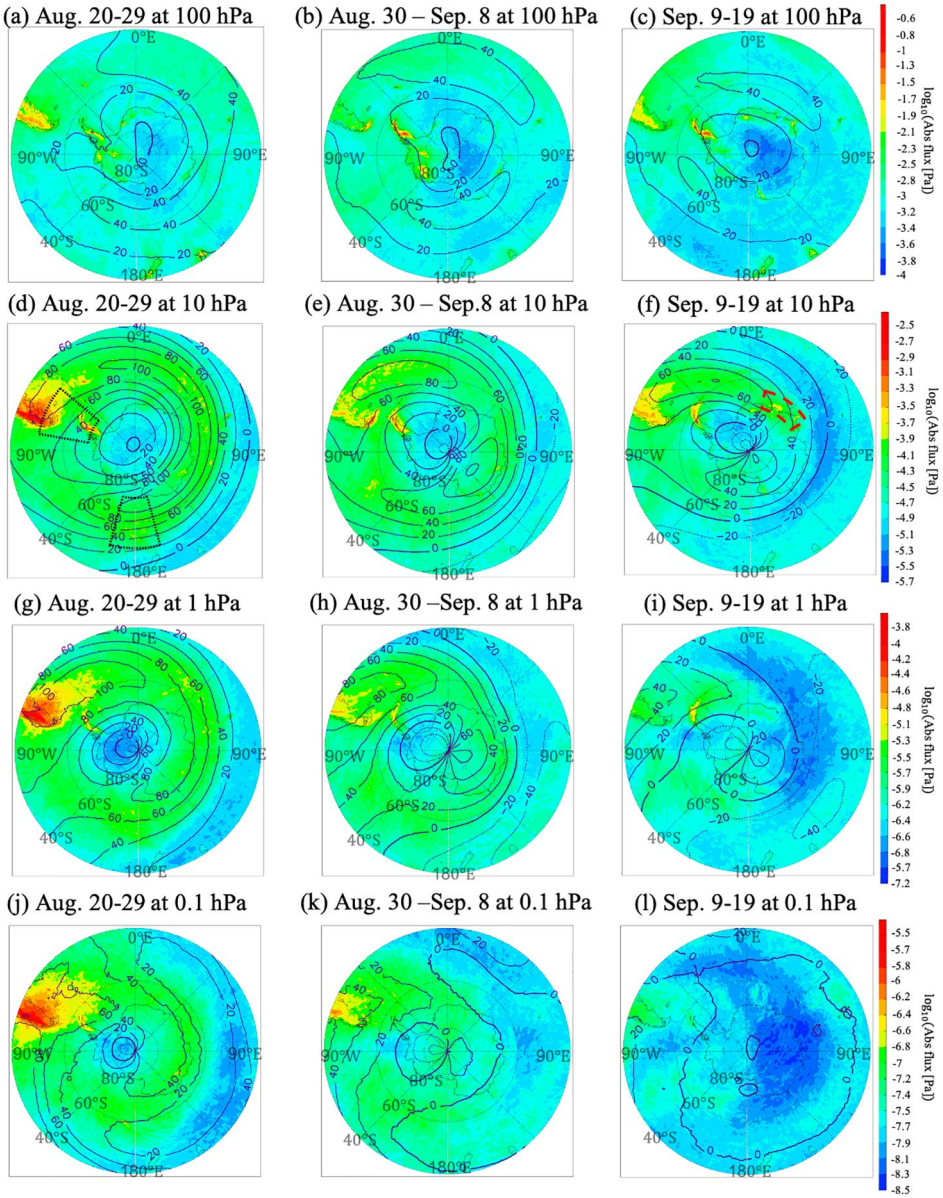

Figure 4. Absolute momentum fluxes averaged in GEOS 5-FP in the three periods: before/after the onset of the 2019 Antarctic stratospheric sudden warming (SSW) (August 20–29 and August 30–September 8), and during the weak zonal wind in the middle/upper stratosphere (September 9–19). The contour lines indicate daily mean zonal wind. Thick lines and dotted lines indicate 0 ms^{-1} and an east wind, respectively. Graphs (a–c) shows the averaged fluxes at 100 hPa. Graphs (d–l) are the same as (a–c), except for 10 hPa (d–f), 1 hPa (g–i), and 0.1 hPa (j–l), respectively. The upper and lower black boxes in (d) indicate the Andes and the Antarctic peninsula and the Ocean region, respectively. The red box in (f) indicate the enhanced activity area due to gravity wave (GW) emitted from the jet.

the fluxes were suppressed because wind reversal filters those GWs from the troposphere that are of small zonal phase speed and the weaking of a stratospheric GW source (the polar night jet). However, the zonal wind during August 30–September 8 over the southern Andes and Antarctic peninsula (Figure 4a) was still strong (40–60 ms^{-1}) at 40–60 km altitudes, that is, the wind reversal filtering and the weakening of a GW source hardly explain this flux decrease during August 30–September 8. Additionally, the flux in the 10–20 km altitudes was larger during August 30–September 8 than that before August 30, which suggested that the orographic source activity was higher. This decrease in flux on August 30 over the southern Andes and Antarctic peninsula could be explained by the wave saturation because of the decrease in the zonal wind. The GWs with westward propagation around the polar night jet tend to have long vertical wavelengths

because of the Doppler shift. When the wind decreases, the vertical wavelengths should likewise decrease. GWs with small vertical wavelengths have a tendency to meet instability conditions, and the growth of the amplitudes is limited (S. A. Alexander et al., 2011; Whiteway et al., 1997). Figures 4c and 4d show the vertical wavelength spectra for the GW relative temperature perturbation and wind over the southern Andes and Antarctic peninsula at 10–70 km from August 20 to August 29, August 30 to September 8, and September 9 to September 19, respectively. The dashed lines indicate a theoretical spectrum in a typical buoyancy frequency ($N^2 = 4 \times 10^{-4}$ s^{-2}). The theoretical spectrum was calculated in accordance with Smith et al. (1987). Figures 4e and 4f show the same values as c and d, except for the ocean region. The spectra were calculated using the Lomb–Scargle method (Scargle, 1982). The power spectral densities (PSDs) over the southern Andes and Antarctic peninsula at vertical wavelengths longer than 20 km dropped to one-half to one-third from August 20–29 to August 30–September 8, although shorter vertical wavelengths than 10 km decreased by less than two-thirds. The characteristic vertical wavelength (local maximum wavelength) also became shorter (~20–~16 km). The PSDs over the ocean dropped to one-half to one-third for all vertical wavelengths, and the characteristic vertical wavelength did not change. This result indicates that the GWs with longer vertical wavelengths were refracted to shorter wavelengths because of the zonal wind weakening after the onset.

5. Summary

We investigated GW variations before and after a rare Antarctic SSW event in 2019 using AIRS, AIM, and GEOS-5 FP, which showed that the GW activity decreased after the SSW onset. This decrease in the GW activity after the onset was probably caused by wind filtering and polar night jet breaking. This GW temporal variation was the same as in the Arctic GWs in vortex displacement minor SSW (Ern et al., 2016) so that the SSW impact on Antarctic GWs is similar to that in the Arctic, at least in the 2019 event. GW activity over the Andes and Antarctic peninsula decreased by half at the SSW onset and the zonal wind weakened, although it was still strong. The weakening of the zonal winds would cause GWs to refract to smaller vertical wavelength and could lead to saturation at lower altitudes. This result implied that the weakening zonal wind suppressed the GW momentum flux by half. Most previous studies regarding the effect of SSWs on GWs emphasized a critical level caused by wind reversal, but our results suggested that the effect of shortening the vertical wavelength cannot be negligible. These effects on the GWs because of the Antarctic SSW should change the GW activity and other phenomena in the upper atmosphere. In particular, this SSW could lower secondary GW excitation altitudes because of a descending primary GW breaking altitude, although GEOS-5 FP cannot resolve this type of secondary GW. Future work will investigate the impact of the decrease of the stratospheric GW on the upper atmosphere during the 2019 SSW.

Data Availability Statement

The AIRS/Aqua gravity wave datasets (Hoffmann et al., 2017) are provided by Forschungszentrum Jülich (https://datapub.fz-juelich.de/slcs/airs/gravity_waves/data). The AIM/CIPS gravity wave datasets are provided by the University of Colorado (http://lasp.colorado.edu/aim/download-data-raa.php). The GEOS-5 FP data were provided by NASA/GMAO (https://portal.nccs.nasa.gov/datashare/gmao/geos-fp/das/).

Acknowledgments
This work was supported by the JSPS grant JRPs-LEAD with the DFG program, JSPS KAKENHI Grant Numbers 19K23465, 18H01270, 18H04446, and 17KK0095, and the Scientific Committee on Antarctic Research (SCAR) fellowship award 2019. J. Yue was supported by NSF grants AGS-1651394, AGS-1834222 and by NASA AIM and 80NSSC20K0628. The authors would like to thank Larry Coy (SSAI and NASA GSFC) for help accessing the GEOS5 FP data, Joan Alexander (NWRA) for providing the AIRS kernel function, Justin Carstens (Virginia Tech) and Cora Randall (CU) for providing the CIPS RAA kernel function. They also helped us to compare the GWs in both GEOS-5 FP and CIPS/AIM.

References

Alexander, M. J. (1998). Interpretations of observed climatological patterns in stratospheric gravity wave variance. *Journal of Geophysical Research*, *103*(D8), 8627–8640. https://doi.org/10.1029/97JD03325

Alexander, M. J., and Grimsdell, A. W. (2013), Seasonal cycle of orographic gravity wave occurrence above small islands in the Southern Hemisphere: Implications for effects on the general circulation, *Journal of Geophysical Research: Atmospheres*, *118*, 11589–11599, https://doi.org/10.1002/2013JD020526

Alexander, S. P., Klekociuk, A. R., & Murphy, D. J. (2011). Rayleigh lidar observations of gravity wave activity in the winter upper stratosphere and lower mesosphere above Davis, Antarctica (69°S, 78°E). *Journal of Geophysical Research*, *116*, D13109. https://doi.org/10.1029/2010JD015164

Aumann, H. H., Chahine, M. T., Gautier, C., Goldberg, M. D., Kalnay, E., McMillin, L. M., et al. (2003). AIRS/AMSU/HSB on the aqua mission: Design, science objectives, data products, and processing systems. *IEEE Transactions on Geoscience and Remote Sensing*, *41*(2), 253–264. https://doi.org/10.1109/tgrs.2002.808356

Bailey, S. M., Thomas, G. E., Rusch, D. W., Merkel, A. W., Jeppesen, C. D., Carstens, J. N., et al. (2009). Phase functions of polar mesospheric cloud ice as observed by the CIPS instrument on the AIM satellite. *Journal of Atmospheric and Solar-Terrestrial Physics*, *71*(3–4), 373–380. https://doi.org/10.1016/j.jastp.2008.09.039

Baldwin, M., Hirooka, T., Oneill, A., & Yoden, S. (2003). Major stratospheric warming in the Southern Hemisphere in 2002: Dynamical aspects of the ozone hole split. *SPARC Newsletter*, *20*, 24–26.

Carstens, J. N., Bailey, S. M., Lumpe, J. D., & Randall, C. E. (2013). Understanding uncertainties in the retrieval of polar mesospheric clouds from the cloud imaging and particle size experiment in the presence of a bright Rayleigh background. *Journal of Atmospheric and Solar-Terrestrial Physics*, *104*, 197–212. https://doi.org/10.1016/j.jastp.2013.08.006

Chahine, M. T., Pagano, T. S., Aumann, H. H., Atlas, R., Barnet, C., Blaisdell, J., et al. (2006). Airs. *Bulletin of the American Meteorological Society*, *87*(7), 911–926. https://doi.org/10.1175/bams-87-7-911

Chandran, A., Collins, R. L., & Harvey, V. L. (2014). Stratosphere-mesosphere coupling during stratospheric sudden warming events. *Advances in Space Research*, *53*(9), 1265–1289. https://doi.org/10.1016/j.asr.2014.02.005

Charlton, A. J., & Polvani, L. M. (2007). A new look at stratospheric sudden warmings. Part I: Climatology and modeling benchmarks. *Journal of Climate*, *20*, 449–469. https://doi.org/10.1175/jcli3996.1

Ern, M., Trinh, Q. T., Kaufmann, M., Krisch, I., Preusse, P., Ungermann, J., et al. (2016). Satellite observations of middle atmosphere gravity wave absolute momentum flux and of its vertical gradient during recent stratospheric warmings. *Atmospheric Chemistry and Physics*, *16*, 9983–10019. https://doi.org/10.5194/acp-16-9983-2016

Fleming, E. L., Chandra, S., Barnett, J. J., & Corney, M. (1990). Zonal mean temperature, pressure, zonal wind and geopotential height as functions of latitude. *Advances in Space Research*, *10*(12), 11–59. https://doi.org/10.1016/0273-1177(90)90386-e

Fritts, D. C., & Alexander, M. J. (2003). Gravity wave dynamics and effects in the middle atmosphere. *Reviews of Geophysics*, *41*, 1003. https://doi.org/10.1029/2001RG0001061

Garcia, R. R., & Boville, B. A. (1994). Downward control" of the mean meridional circulation and temperature distribution of the polar winter stratosphere. *Journal of the Atmospheric Sciences*, *51*, 2238–2245. https://doi.org/10.1175/1520-0469(1994)051<2238:COTMMC>2.0.CO;2

Gelaro, R., McCarty, W., Suárez, M. J., Todling, R., Molod, A., Takacs, L., et al. (2017). The modern-era retrospective analysis for research and applications, Version 2 (MERRA-2). *Journal of Climate*, *30*, 5419–5454. https://doi.org/10.1175/jcli-d-16-0758.1

Geller, M. A., Love, M. J. P. T., Bacmeister, J., Ern, M., Hertzog, A., Manzini, E., et al. (2013). A comparison between gravity wave momentum fluxes in observations and climate models. *Journal of Climate*, *26*, 6383–6405. https://doi.org/10.1175/jcli-d-12-00545.1

Hendricks, E. A., Doyle, J. D., Eckermann, S. D., Jiang, Q., & Reinecke, P. A. (2014). What is the source of the stratospheric gravity wave belt in austral winter? *Journal of the Atmospheric Sciences*, *71*, 1583–1592. https://doi.org/10.1175/jas-d-13-0332.1

Hoffmann, L., Grimsdell, A. W., & Alexander, M. J. (2016). Stratospheric gravity waves at Southern Hemisphere orographic hotspots: 2003-2014 AIRS/Aqua observations. *Atmospheric Chemistry and Physics*, *16*, 9381–9397. https://doi.org/10.5194/acp-16-9381-2016

Hoffmann, L., Spang, R., Orr, A., Alexander, M. J., Holt, L. A., & Stein, O. (2017). A decadal satellite record of gravity wave activity in the lower stratosphere to study polar stratospheric cloud formation. *Atmospheric Chemistry and Physics*, *17*(4), 2901–2920. https://doi.org/10.5194/acp-17-2901-2017

Hoffmann, L., Xue, X., & Alexander, M. J. (2013). A global view of stratospheric gravity wave hotspots located with atmospheric infrared sounder observations. *Journal of Geophysical Research: Atmospheres*, *118*, 416–434. https://doi.org/10.1029/2012jd018658

Holt, L. A., Alexander, M. J., Coy, L., Liu, C., Molod, A., Putman, W., & Pawson, S. (2017). An evaluation of gravity waves and gravity wave sources in the Southern Hemisphere in a 7 km global climate simulation. *Quarterly Journal of the Royal Meteorological Society*, *143*, 2481–2495. https://doi.org/10.1002/qj.3101

Holt, L. A., Alexander, M. J., Coy, L., Molod, A., Putman, W., & Pawson, S. (2016). Tropical waves and the quasi-biennial oscillation in a 7-km global climate simulation. *Journal of the Atmospheric Sciences*, *73*, 3771–3783. https://doi.org/10.1175/jas-d-15-0350.1

Jewtoukoff, V., Hertzog, A., Plougonven, R., Cámara, A. D. L., & Lott, F. (2015). Comparison of gravity waves in the Southern Hemisphere derived from balloon observations and the ECMWF analyses. *Journal of the Atmospheric Sciences*, *72*, 3449–3468. https://doi.org/10.1175/jas-d-14-0324.1

Jia, Y., Zhang, S., Yi, F., Huang, C., Huang, K., Gan, Q., & Gong, Y. (2015). Observations of gravity wave activity during stratospheric sudden warmings in the Northern Hemisphere. *Science China Technological Sciences*, *58*, 951–960. https://doi.org/10.1007/s11431-015-5806-3

Lindzen, R. S. (1981). Turbulence and stress owing to gravity wave and tidal breakdown. *Journal of Geophysical Research*, *86*(C10), 9707–9714. https://doi.org/10.1029/JC086iC10p09707

Lucchesi, R. (2013). File specification for GEOS-5 FP. *Tech. Rep. GMAO Off. Note No. 4. (Version 1.0)*. Retrieved from https://ntrs.nasa.gov/search.jsp?R=20150001437

Matthewman, N. J., Esler, J. G., Charlton-Perez, A. J., & Polvani, L. M. (2009). A new look at stratospheric sudden warmings. Part III: Polar vortex evolution and vertical structure. *Journal of Climate*, *22*, 1566–1585. https://doi.org/10.1175/2008jcli2365.1

McClintock, W. E., Rusch, D. W., Thomas, G. E., Merkel, A. W., Lankton, M. R., Drake, V. A., et al. (2009). The cloud imaging and particle size experiment on the Aeronomy of Ice in the mesosphere mission: Instrument concept, design, calibration, and on-orbit performance. *Journal of Atmospheric and Solar-Terrestrial Physics*, *71*(3–4), 340–355. https://doi.org/10.1016/j.jastp.2008.10.011

McFarlane, N. A. (1987). The effect of orographically excited gravity wave drag on the general circulation of the lower stratosphere and troposphere. *Journal of the Atmospheric Sciences*, *44*, 1775–1800. https://doi.org/10.1175/1520-0469(1987)044<1775:teooeg>2.0.co;2

Murphy, D. J., Alexander, S. P., Klekociuk, A. R., Love, P. T., & Vincent, R. A. (2014). Radiosonde observations of gravity waves in the lower stratosphere over Davis, Antarctica. *Journal of Geophysical Research: Atmospheres*, *119*, 11973–11996. https://doi.org/10.1002/2014JD022448

Plougonven, R., & Zhang, F. (2014). Internal gravity waves from atmospheric jets and fronts. *Reviews of Geophysics*, *52*, 33–76. https://doi.org/10.1002/2012RG000419

Preusse, P., Eckermann, S. D., Ern, M., Oberheide, J., Picard, R. H., Roble, R. G., et al. (2009). Global ray tracing simulations of the SABER gravity wave climatology. *Journal of Geophysical Research*, *114*, D08126. https://doi.org/10.1029/2008JD011214

Randall, C. E., Carstens, J., France, J. A., Harvey, V. L., Hoffmann, L., Bailey, S. M., et al. (2017). New AIM/CIPS global observations of gravity waves near 50-55 km. *Geophysical Research Letters*, *44*, 7044–7052. https://doi.org/10.1002/2017GL073943

Ratnam, M. V., Tetzlaff, G., & Jacobi, C. (2004). Global and seasonal variations of stratospheric gravity wave activity deduced from the CHAMP/GPS satellite. *Journal of the Atmospheric Sciences*, *61*, 1610–1620. https://doi.org/10.1175/1520-0469(2004)061<1610:gasvos>2.0.co;2

Rusch, D., Thomas, G., Merkel, A., Olivero, J., Chandran, A., Lumpe, J., et al. (2017). Large ice particles associated with small ice water content observed by AIM CIPS imagery of polar mesospheric clouds: Evidence for microphysical coupling with small-scale dynamics. *Journal of Atmospheric and Solar-Terrestrial Physics*, *162*, 97–105. https://doi.org/10.1016/j.jastp.2016.04.018

Sato, K., & Yoshiki, M. (2008). Gravity wave generation around the polar vortex in the stratosphere revealed by 3-hourly radiosonde observations at Syowa Station. *Journal of the Atmospheric Sciences*, *65*(12), 3719–3735.Retrieved Dec. 29, 2020. https://doi.org/10.1175/2008JAS2539.1

Scargle, J. D. (1982). Studies in astronomical time series analysis. II - Statistical aspects of spectral analysis of unevenly spaced data. *Acta Pathologica Japonica*, *263*, 835–853. https://doi.org/10.1086/160554

Smith, S. A., Fritts, D. C., & Vanzandt, T. E. (1987). Evidence for a saturated spectrum of atmospheric gravity waves. *Journal of the Atmospheric Sciences*, *44*(10), 1404–1410. https://doi.org/10.1175/1520-0469(1987)044<1404:efasso>2.0.co;2

Thurairajah, B., Bailey, S. M., Cullens, C. Y., Hervig, M. E., & Russell, J. M., III (2014). Gravity wave activity during recent stratospheric sudden warming events from SOFIE temperature measurements. *Journal of Geophysical Research: Atmospheres*, *119*, 8091–8103. https://doi.org/10.1002/2014JD021763

Wang, L., & Alexander, M. J. (2009). Gravity wave activity during stratospheric sudden warmings in the 2007-2008 Northern Hemisphere winter. *Journal of Geophysical Research*, *114*, D18108. https://doi.org/10.1029/2009JD011867

Whiteway, J. A., Duck, T. J., Donovan, D. P., Bird, J. C., Pal, S. R., & Carswell, A. I. (1997). Measurements of gravity wave activity within and around the Arctic stratospheric vortex. *Geophysical Research Letters*, *24*(11), 1387–1390. https://doi.org/10.1029/97GL01322

Wright, C. J., Osprey, S. M., Barnett, J. J., Gray, L. J., & Gille, J. C. (2010). High resolution dynamics limb sounder measurements of gravity wave activity in the 2006 Arctic stratosphere. *Journal of Geophysical Research*, *115*, D02105. https://doi.org/10.1029/2009JD011858

Yamashita, C., England, S. L., Immel, T. J., & Chang, L. C. (2013). Gravity wave variations during elevated stratopause events using SABER observations. *Journal of Geophysical Research: Atmospheres*, *118*, 5287–5303. https://doi.org/10.1002/jgrd.50474

Yamashita, C., Liu, H.-L., & Chu, X. (2010). Gravity wave variations during the 2009 stratospheric sudden warming as revealed by ECMWF-T799 and observations. *Geophysical Research Letters*, *37*, L22806. https://doi.org/10.1029/2010GL045437

Yamazaki, Y., Matthias, V., Miyoshi, Y., Stolle, C., Siddiqui, T., Kervalishvili, G., et al. (2020). September 2019 Antarctic sudden stratospheric warming: Quasi-6-day wave burst and ionospheric effects. *Geophysical Research Letters*, *47*, e2019GL086577. https://doi.org/10.1029/2019gl086577